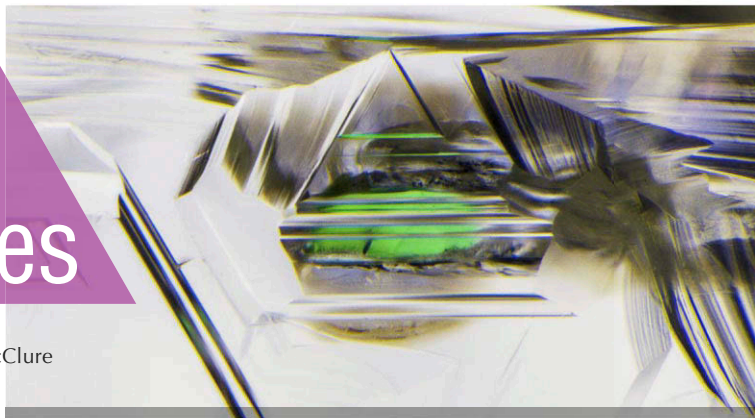


# Lab Notes

## Editors

Thomas M. Moses | Shane F. McClure



## Dramatic Color Zoning in ALEXANDRITE

An 8.55 ct alexandrite was recently submitted to GIA's Bangkok laboratory. Standard gemological testing yielded a refractive index of 1.745–1.754 and a specific gravity of 3.73. The stone displayed a change of color from green in daylight to reddish purple in incandescent light (figure 1). All of these properties were consistent with alexandrite.

Microscopic examination revealed natural fingerprints, needles, zoned particles, and color zoning, along with internal growth features. Interestingly, the stone showed a thin color zone very close to some of the pavilion facets and culet when immersed in methylene iodide (figure 2).

Testing with a handheld spectroscope and ultraviolet-visible (UV-Vis) spectroscopy revealed chromium ( $\text{Cr}^{3+}$ ) features. The absorption feature assigned to  $\text{Cr}^{3+}$  was located at 680 nm, with a broad band around 589 nm (figure 3). In contrast, when examined from the side (girdle to girdle), no  $\text{Cr}^{3+}$  feature was detected. This confirmed that color zoning at the culet strongly affected the color of this stone and its color-change effect.

The cutter designed the gem to contain the thin color zone along the pavilion facets and culet to display a

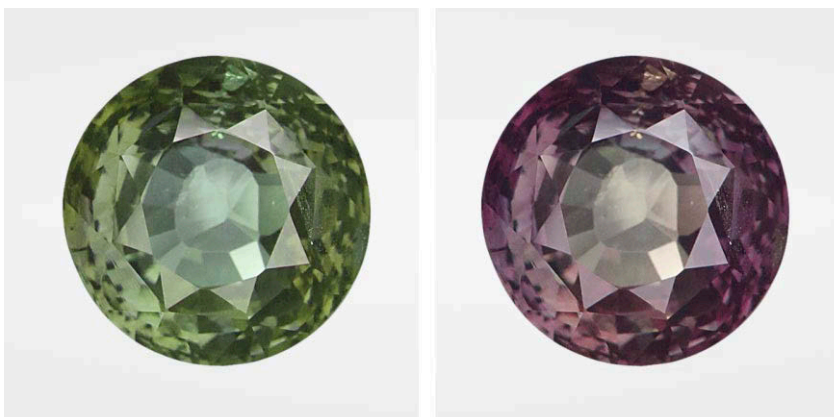


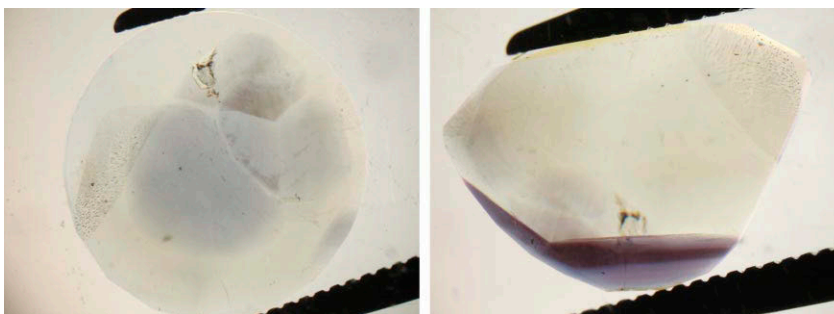
Figure 1. The 8.55 ct alexandrite in daylight (left) and incandescent light (right).

color change when viewed face-up. Without the  $\text{Cr}^{3+}$ -containing color zone, this stone would be chrysoberyl.

This example illustrates that orienting a color zone with the right trace elements combined with proper cutting can affect the variety designation of a gem.

*Vararut Weeramongkhonlert*

Figure 2. Viewed in immersion, the alexandrite displayed color zoning when viewed table-down (left) and from the side (right); field of view 12.5 mm.



## Novelty Cut DIAMOND with Remarkable “Fire and Ice” Fluorescence

A 0.37 ct Fancy yellowish brown diamond (figure 4, left) was recently submitted to the Carlsbad laboratory for Color Origin and Identification service. This novelty cut, faceted to resemble a dagger or sword, was

*Editors' note: All items were written by staff members of GIA laboratories.*

GEMS & GEMOLOGY, Vol. 56, No. 3, pp. 416–425.

© 2020 Gemological Institute of America

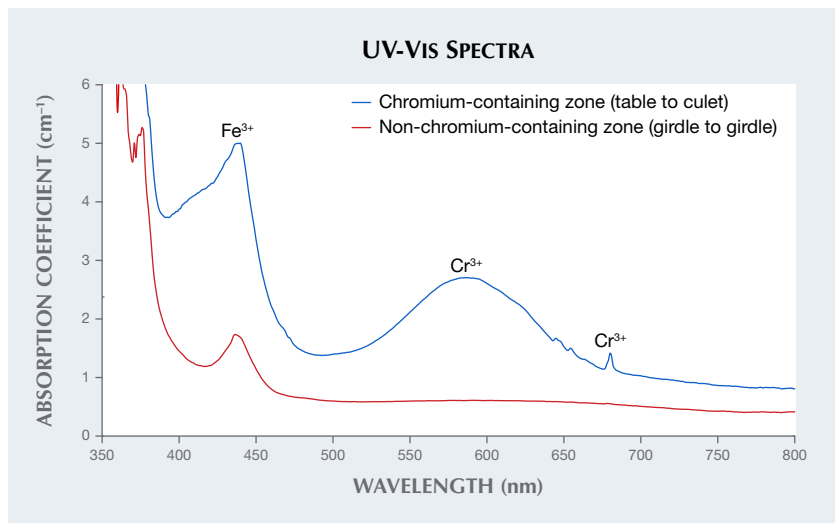


Figure 3. UV-Vis absorption spectra of the alexandrite from table to culet (chromium-bearing color zone) and girdle to girdle (non-chromium-bearing color zone).

remarkable for its well-defined hydrogen-rich and cape regions, which created a distinctive fluorescence pattern. The “blade” section of the diamond fluoresced a strong yellow color, while the “hilt” fluoresced a strong blue (figure 4, right). As a result, we thought this diamond was an interesting interpretation of a lightsaber.

Microscopic examination showed that throughout the yellow-fluoresc-

ing area were cloud inclusions, consisting of a high density of light-scattering micro-inclusions that correlate strongly with the presence of hydrogen. These are often called “hydrogen clouds” due to their coincidence with notable concentrations of hydrogen-related defects (W. Wang and W. Mayerson, “Symmetrical clouds in diamond—the hydrogen connection,” *Journal of Gemmology*, Vol. 28, No. 3, 2002, pp. 143–152).

Figure 5. The infrared absorption spectra of this type Ia diamond show weak hydrogen bands in the “hilt” (blue line) and high hydrogen content in the “blade” (yellow line). The spectra are stacked for clarity.

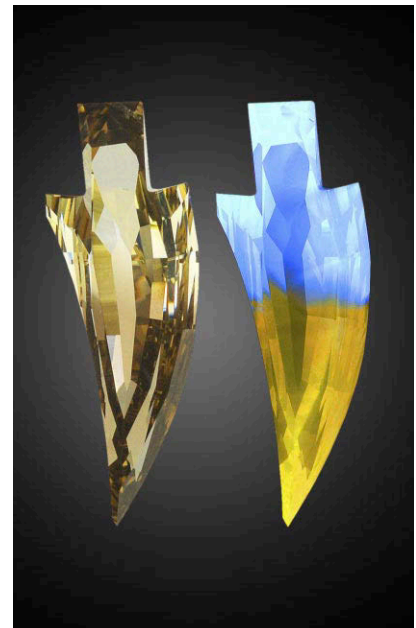
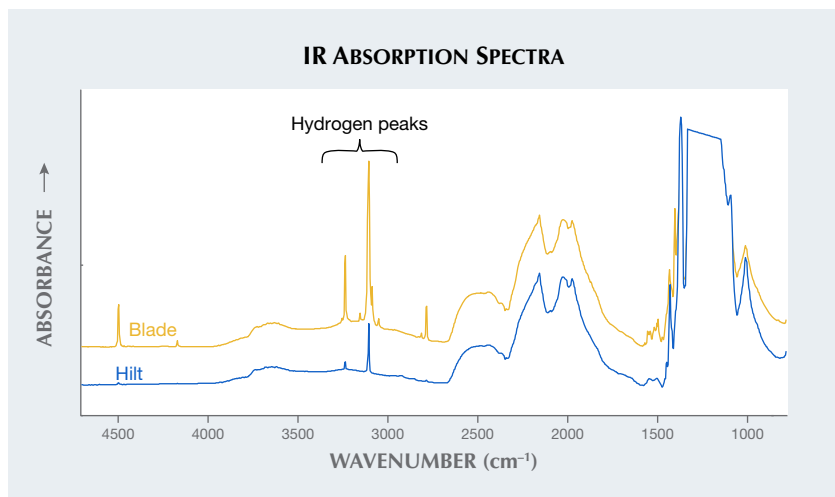


Figure 4. This 0.37 ct Fancy yellowish brown diamond (left) contained a remarkable hydrogen cloud in the “blade” and cape features in the “hilt.” The stone showed corresponding areas of yellow and blue fluorescence in long-wave UV (right).

The infrared absorption spectra showed a type Ia diamond with saturated concentrations of nitrogen. Spectra recorded from the individual sectors were consistent with the gemological observations, as the yellow-fluorescing section containing the “hydrogen clouds” did show significantly more hydrogen than the blue-fluorescing area (figure 5).

To better understand the defects creating the dramatic difference in both the observable color in daylight and the fluorescence color under long-wave UV (figure 6), we performed photoluminescence (PL) mapping using 455 and 532 nm excitation at liquid nitrogen temperatures. The maps revealed distinct differences between the two areas. The yellow-fluorescing area showed peaks at 603 nm, a doublet at 641 and 645 nm, and a strong peak at 700.5 nm in the 532 nm PL spectra (figure 7). These peaks

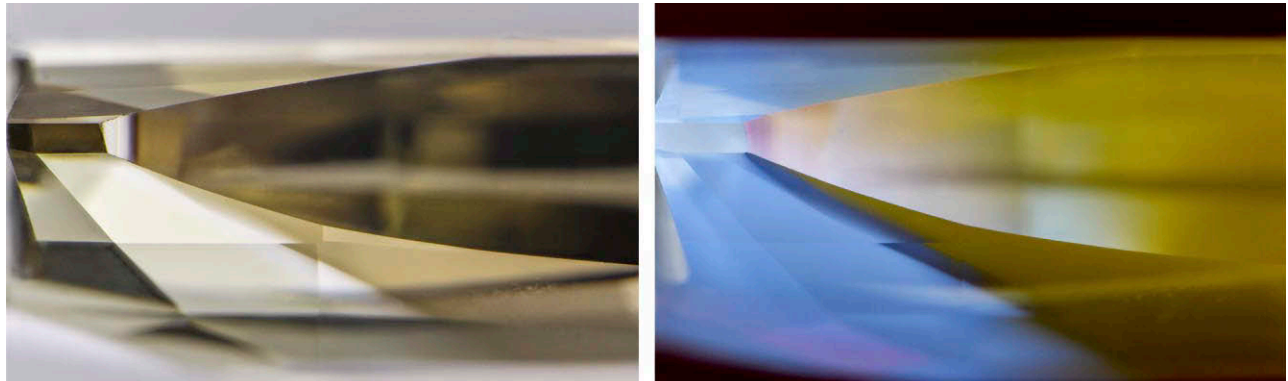


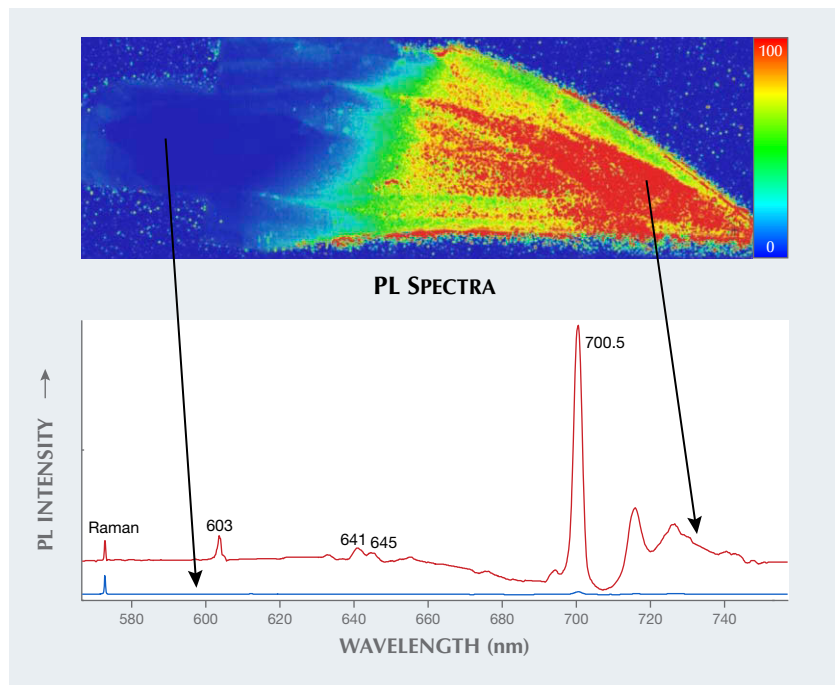
Figure 6. The distinctive separation line between the light yellowish brown cape section and the brown hydrogen section (left) matches the boundary between the blue and yellow fluorescence under long-wave UV (right); field of view 3.59 mm.

have all been ascribed to nickel and are often seen in hydrogen-rich diamonds (K. Iakoubovskii and G.J. Adriaenssens, "Optical characterization of natural Argyle diamonds," *Diamond*

*and Related Materials*, Vol. 11, No. 1, 2002, pp. 125–131; S. Eaton-Magaña et al., "Inclusion and point defect characteristics of Marange graphite-bearing diamonds after high tempera-

ture annealing," *Diamond and Related Materials*, Vol. 71, 2017, pp. 20–29). The blue-fluorescing area only shows a very small peak at 700.5 nm in the 532 nm PL map.

Figure 7. Top: This PL map shows the false-color intensity of the 700.5 nm peak area (ratioed to the diamond Raman peak) using 532 nm excitation at liquid nitrogen temperature; this feature ascribed to Ni is concentrated within the yellow-fluorescing area of the diamond. Field of view 9.2 mm. Bottom: Representative PL spectra from the "blue" and "red" regions of the 532 nm PL map. The lines are stacked for clarity, and the diamond Raman peak intensities (573 nm) are scaled equivalently.



For PL spectra collected at 325 nm excitation, the N3 center is the major feature within the blue-fluorescing area, while a broad band centered at ~550 nm dominates the yellow-fluorescing area (figure 8). Also detected were peaks at 488 nm (ascribed to nickel; I.A. Dobrinets et al., *HPHT-Treated Diamonds*, Springer, 2013), 522 nm (unassigned), and the 603 and 700.5 nm peaks mentioned above. The yellow-fluorescing area also showed elevated intensities of the 490.7 nm peak (a natural feature in type Ia diamonds) in the 455 nm PL map and peaks at 926 and 948 nm (features also often seen in diamonds enriched with hydrogen and nickel; Eaton-Magaña et al., 2017) in the 830 nm excitation PL spectra.

Gemological and spectroscopic examination yielded interesting features such as this diamond's two distinct growth chemistries. The blue-fluorescing area had few inclusions and the typical fluorescence and PL spectroscopy of a cape diamond. The yellow-fluorescing side had higher hydrogen-related peaks in the infrared, hydrogen cloud inclusions, and pronounced nickel-related peaks in the PL spectra that are often seen in hydrogen-rich diamonds.



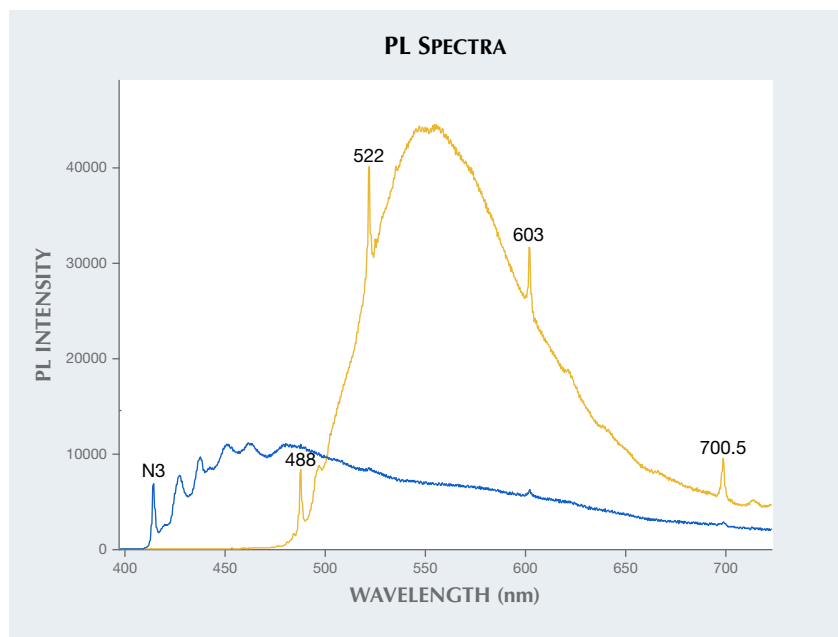


Figure 8. These two PL spectra were collected with 325 nm excitation at liquid nitrogen temperature from the blue- and yellow-fluorescing regions. Due to limitations of the optics, we were unable to collect the diamond Raman peak along with the visible range luminescence; however, the two spectra were collected with the same laser power and plotted on the same scale.

The cutting style of this diamond, while unconventional, served to showcase the remarkable fluorescence scene illuminated within. The fluorescence differences allow this diamond to be imagined as a lightsaber or a sword of fire and ice.

Maryam Mastery Salimi and  
Sally Eaton-Magaña

### Color-Change Cat's-Eye DIASPORE

A 60.71 ct cabochon was recently submitted to the Tokyo lab for identification (figure 9). Diaspore,  $\alpha$ -AlO(OH), is one of the main aluminum minerals in bauxites, along with gibbsite,  $\gamma$ -Al(OH)<sub>3</sub>, and boehmite,  $\gamma$ -AlO(OH). It is often observed as inclusions in rubies. Diaspore is also a gem in its own right, although it is very brittle and has perfect cleavage. The birefringence blink method revealed refractive indices of 1.69 and 1.74 and that the stone was biaxial. A dichroscope revealed strong trichroism: yellowish green, purple, and brown. The Raman spectrum was

consistent with diaspore in the RRUFF reference database (R060287).

The hue of this stone changed from greenish yellow under daylight or fluorescent light to pinkish brown under incandescent light. Diaspore's color change can be caused by the chromophores Cr<sup>3+</sup>, V<sup>3+</sup>, and Fe<sup>2+</sup>-Ti<sup>4+</sup> pairs (C. Shen and R. Lu, "The color origin of gem diaspore: Correlation to corundum," Winter 2018 *G&G*, pp.



Figure 9. The 60.71 ct diaspore displaying color change and chatoyancy under fluorescent light (left) and incandescent light (right).

394–403). Color-change diaspores are sometimes known in the trade as "Zultanite" or "Csarite."

Chatoyant phenomena are usually the result of many long, thin, and closely spaced parallel needles or fibers, combined with cutting of a cabochon in the correct orientation to optimize the reflection of light off of these parallel inclusions. In this stone, the chatoyancy was caused not only by needles and/or tubes but also by the combination of iridescent reflective thin films or fissures in various shapes from ultrafine to wide, aligned along repeated cleavages (figure 10). Although some fissures reached the surface, no clarity

Figure 10. Needles and/or tubes with iridescent reflective thin films or fissures producing chatoyancy under brightfield and overhead illumination (left) and overhead illumination only (right); field of view 13.60 mm.

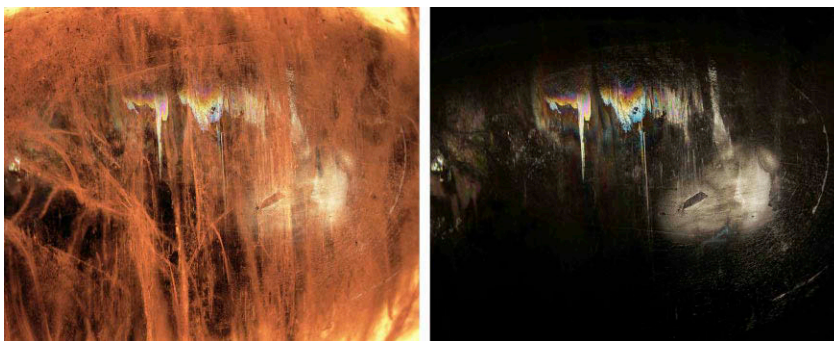




Figure 11. The red dashed line follows the edges of a large quartz crystal found breaking the surface of this 2.98 ct emerald.

enhancement was detected in this diaspore.

Taku Okada

### EMERALD with Large Quartz Inclusion

A 2.98 ct emerald with a large, surface-reaching quartz inclusion was recently examined at the Carlsbad laboratory. The inclusion followed the red dashed outline shown in figure 11.

The discovery was made upon taking a refractive index reading on

the table of the emerald. As the stone was rotated on the hemicylinder of the refractometer, the reading alternated between 1.581–1.590 and 1.545–1.550, typical refractive indexes for emerald and quartz, respectively. Upon microscopic inspection, a large colorless crystal was seen breaking the crown surface of the stone. This inclusion was further documented via photomicrography using both reflected and transmitted light (figure 12). The colorless crystal was conclusively identified by Raman spectroscopy as quartz. Raman spectroscopy also revealed the identity of the abundant acicular crystals seen throughout the emerald as actinolite.

Quartz inclusions within emerald are not commonly seen but have been reported in the gemological literature. In the *Photoatlas of Inclusions in Gemstones*, Volume 3, by E.J. Gübelin and J.I. Koivula (2008), they are listed as possible inclusions found in emeralds from Brazil, Colombia, Russia, and Tanzania. Quartz has also been seen within Madagascar emeralds. This example shows the value of simple standard gemological instruments, such as the refractometer and microscope, as a means to help identify unusual inclusions.

Britni LeCroy

### 15.53 ct PEARL Discovered in Edible Oyster from the Ostreidae Family

A white, non-nacreous baroque pearl weighing 15.53 ct and measuring  $19.54 \times 13.26 \times 11.57$  mm (figure 13) was recently submitted to GIA's Carlsbad laboratory for examination. Information from previously observed non-nacreous pearls submitted to GIA suggested the pearl was of scallop origin—a member of the Pectinidae family. The supporting evidence included a calcite peak seen at  $280 \text{ cm}^{-1}$  with associated peaks at 712, 1085, and  $1437 \text{ cm}^{-1}$  in the Raman spectrum, combined with a patchy surface appearance. Additionally, energy-dispersive X-ray fluorescence (EDXRF) chemical analysis showed low levels of manganese (Mn), confirming a saltwater growth environment. Real-time microradiography (RTX) revealed its natural formation, with a growth arc structure that followed the pearl's overall shape and a rounded, slightly less radio-opaque core (figure 14).

The client later informed the laboratory that the pearl had been found in an edible oyster while eating at a restaurant. Unfortunately, the host shell had not been retained and no photographs had been taken upon initial discovery. Despite this, the client

Figure 12. Left: The subtle luster difference reveals a relatively large quartz crystal inclusion and quartz veins breaking the table of the emerald host in reflected light. Right: The quartz crystal was also viewed in transmitted light, although less visible contrast was noted. Field of view (left and right) 7.19 mm.

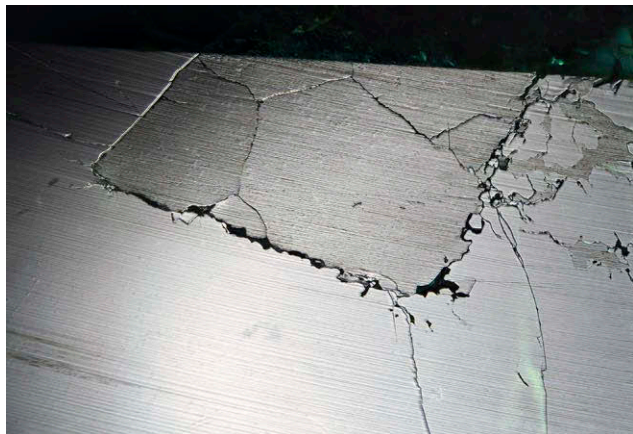






Figure 13. A white non-nacreous pearl weighing 15.53 ct and measuring  $19.54 \times 13.26 \times 11.57$  mm was found in an edible oyster, a member of the *Ostreidae* family.

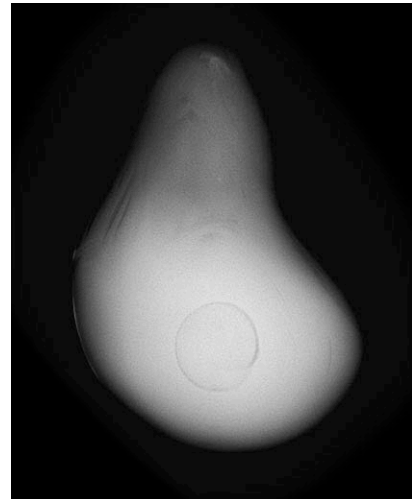


Figure 14. RTX imaging revealed a growth arc structure surrounding a rounded core of less radio-opacity, indicating the pearl formed naturally.

later returned to the restaurant to obtain shells from the two types of oysters served on their menu, the Pacific oyster (*Crassostrea gigas*) and the Atlantic oyster (*Crassostrea virginica*). Gemologists were able to use these shells to gather additional gemological information and compare the results to the submitted pearl.

Raman spectroscopic analysis verified that the shells were composed of calcite, and visual inspection showed nondirectional patches of a broad, mottled cellular structure bearing a

striking resemblance to the pearl. However, these qualities are also seen in some white scallop pearls, as it is possible for them to contain a patchwork of directionless cells. A strong contrast, though, was seen in the microscopic surface appearance. The cellular structure within the oyster shells exhibited a slight reflective colored sheen in certain orientations when illuminated by a fiber-optic light, creating a faint iridescent phenomenon. This characteristic was nearly identical to the surface appear-

ance of the pearl under examination (figure 15, left and center). Conversely, the individual cells of scallop pearls had a fibrous structure, and light reflected from them produced a shimmering sheen or silky appearance. This appearance has been noted to be a unique feature of scallop pearls in the literature (K. Scarratt and H.A. Hänni, "Pearls from the lion's paw scallop," *Journal of Gemmology*, Vol. 29, No. 4, 2004, pp. 193–203), and an example is shown in figure 15 (right). Such features were not observed on

Figure 15. Left: A microscopic view of the shell revealed a directionless patchwork of cells with an unstructured opaque white patch. The cells exhibited a faint iridescent phenomenon when illuminated by a fiber-optic light in certain orientations; field of view 9.87 mm. Center: A nearly identical appearance can be seen on the surface of the pearl; field of view 7.19 mm. Right: A differing mosaic pattern of non-oriented cells displayed on the surface of a white scallop pearl. Each cell contains a fibrous structure, and reflected light produced a unique shimmering sheen or silky appearance; field of view 5.08 mm.





Figure 16. Left: An overall patchy or mosaic pattern on the surface of the pearl; field of view 13.45 mm. Right: A similar appearance on the surface of a LaPearlite cabochon fashioned from an oyster shell; field of view 14.52 mm.

the surface of the pearl under examination or the oyster shells.

The pearl and oyster shells also displayed translucency over most of their surfaces with randomly oriented opaque white patches. The cellular patchwork formation was faint or absent in these white patchy areas. This characteristic further supported their relationship (again, see figure 15, left and center).

Moreover, the angular mosaic-like appearance with areas of soft iridescence seen on the pearl closely resembled the surface of previously observed “LaPearlite” cabochons fashioned from oyster shells (figure 16; see also Summer 2018 Lab Notes, pp. 213–214). Lastly, it was also noted that the pearl, oyster shells, and LaPearlite samples all possessed layers of yellowish organic material covering part of their surfaces.

With supporting surface evidence from the oyster shells and the previously examined LaPearlite cabochon samples, gemologists were able to conclude that the pearl originated from the Ostreidae family, an edible oyster rather than a species of scallop, or member of the Pectinidae family. A few oyster pearls have been previously recorded in the literature [C.P. Idyll, “The pearls of Margarita,” *Americas*, Vol. 19, No. 8, 1967, pp. 8–14; K. Scarratt et al., “A note on a pearl attached to the interior of *Crasostrea virginica* (Gmelin, 1791) (an edible oyster, common names, American or Eastern oyster),” *Journal of Gemmology*, Vol. 30, No. 1/2, 2006, pp. 43–50; Fall 2019 Gem News International, pp. 439–440].

Yet this is the first examination by GIA gemologists of a pearl known to have been produced from the Ostreidae family (true oyster) mollusk, as well as the first GIA pearl identification report for one. Additionally, the significant size and weight of this 15.53 ct pearl are noteworthy. Although oyster pearls are not of prime importance within the global pearl market, they are rare, curious novelties that can offer insight to the scientific pearl community.

*Britni LeCroy and  
Artitaya Homkrajae*

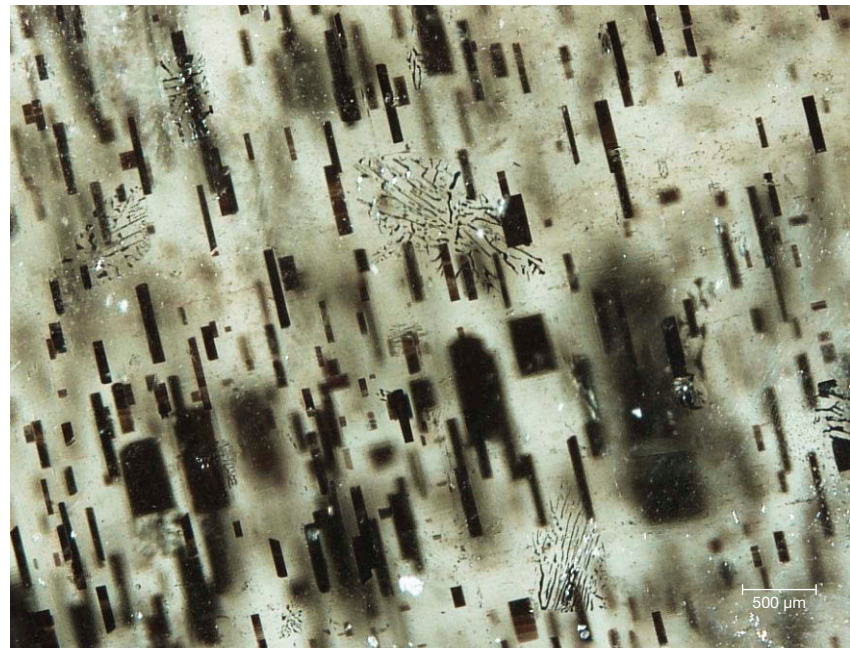


Figure 17. This 2.71 ct star peridot contained numerous magnetite inclusions.

### Magnetite Inclusions in Star PERIDOT

The Tokyo lab received a transparent yellow-green peridot displaying four-rayed asterism (figure 17). The 2.71 ct stone, measuring 9.94 × 7.88 × 4.08 mm, was reportedly from Myanmar. It had a spot refractive index of 1.64 and an SG of 3.29 and was identified as terrestrial peridot, which can be

Figure 18. The star peridot contained rectangular to needle-like magnetite inclusions responsible for the four-rayed asterism; field of view 2.50 mm.





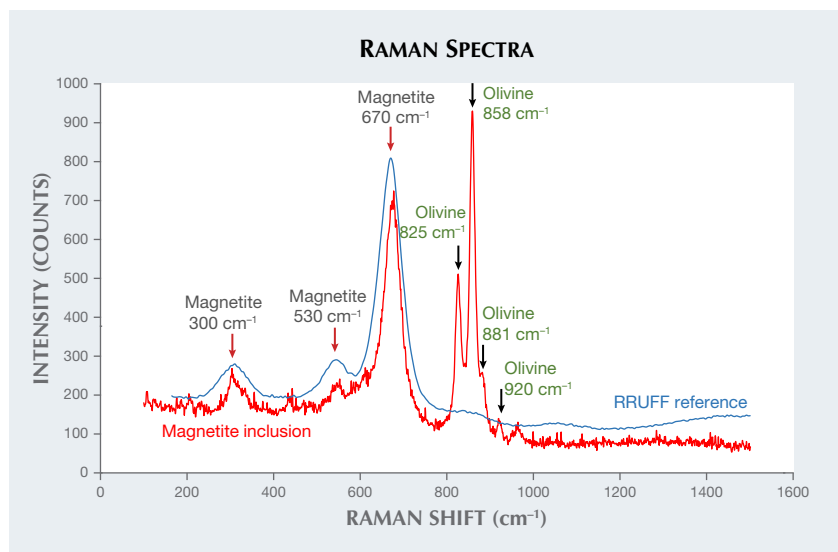


Figure 19. Raman spectrum of the magnetite platelet/needle inclusion in the star peridot, compared with a magnetite Raman spectrum (R080025) from the RRUFF database.

distinguished from pallasitic peridot by trace element concentrations.

The asterism of this stone was created by light reflecting from dark, rectangular platelets and needles (figure 18), which were visible without magnification. These were identified as magnetite by Raman spectroscopy (figure 19), namely the three broad bands at around 300, 530, and 670  $\text{cm}^{-1}$  (e.g., O.N. Shebanova and P. Lazor, "Raman spectroscopic study of magnetite ( $\text{FeFe}_2\text{O}_4$ ): A new assignment for the vibrational spectrum," *Journal of Solid State Chemistry*, Vol. 174, No. 2, 2003, pp. 424–430), and its reaction to a magnet. These inclusions conforming to one crystallographic plane of the peridot were exsolution lamellae, which are interpreted to have formed by the exsolution of an iron-oxide component from the host peridot (olivine) by subsolidus reaction during cooling and/or decompression. (e.g., R.Y. Zhang et al., "Magnetite lamellae in olivine and clinohumite from Dabie UHP ultramafic rocks, central China," *American Mineralogist*, Vol. 84, No. 4, 1999, pp. 564–569). The inclusions in this peridot were larger and seemed to have a different shape from those in previously reported Burmese peridot (Spring 2020 Gems News International, pp. 159–160), which were more

acicular. Similar inclusions within a star peridot were also reported (Summer 2009 Lab Notes, pp. 138–139) but could not be identified by Raman spectroscopy due to interference from the host peridot. Although magnetite inclusions have been found in olivines (the mineralogical term for peridot) within some ultramafic and metamorphic rocks by petrological and mineralogical studies (e.g., Zhang

Figure 20. This 29.59 ct spodumene with light blue color is quite rare. It has been reported that exposure to sunlight changes this color to pink or purple.



et al., 1999), it is notable that magnetite exsolution lamellae were identified in this star peridot using a Raman spectrometer. The difference in shape and size of the inclusions, however, could be due to the duration of the actual cooling and/or decompression time from the formation of the stone to its emplacement on the earth's surface. A longer emplacement time usually allows a longer time for the inclusions to grow larger.

Masumi Saito and Makoto Miura

### Blue SPODUMENE

Recently this contributor received a light aqua blue stone that unexpectedly turned out to be spodumene. The following gemological properties were recorded for this 29.59 ct oval modified brilliant (figure 20): refractive indices of 1.661 and 1.676, birefringence of 0.015, a biaxial optic figure, and hydrostatic specific gravity of approximately 3.20. Pleochroism was observed using a linear polarizing filter, which revealed blue, yellowish green, and colorless trichroism. The RI and SG values were consistent with those reported for spodumene in the gemological literature. Magnification of this



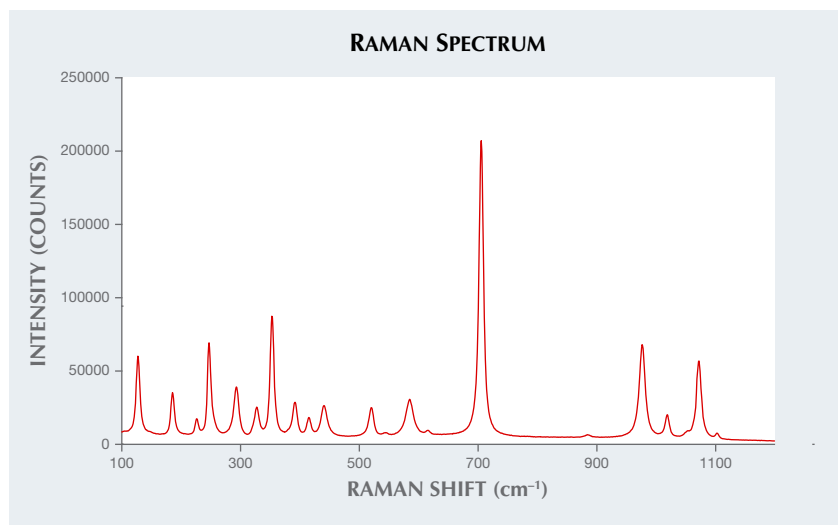
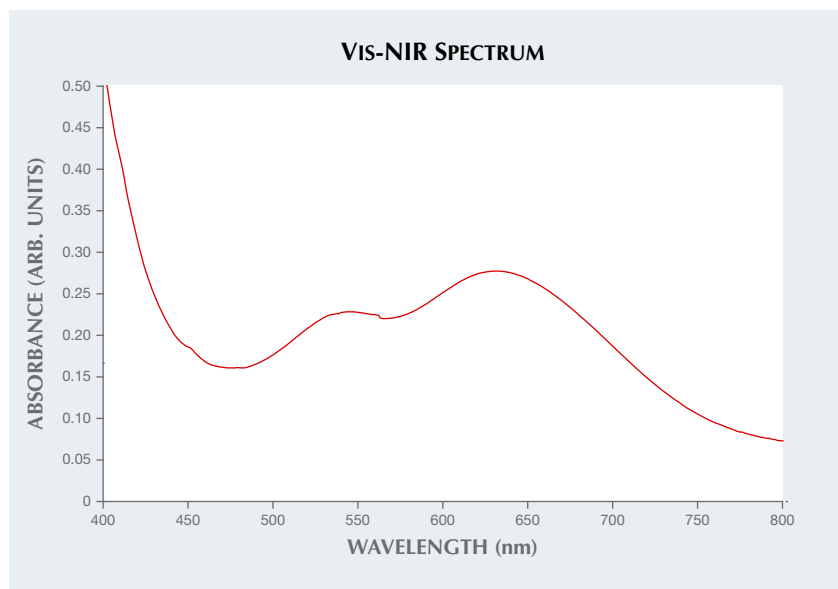


Figure 21. The light blue stone's Raman spectrum was consistent with that of spodumene published in the RRUFF database (R040050).

lithium aluminum silicate ( $\text{LiAlSi}_2\text{O}_6$ ) showed parallel growth features, ripple-like internal graining, and most importantly two cleavage planes along the girdle edge. The identity of the stone was confirmed by further advanced testing. Its Raman spectrum (figure 21), with reference to the RRUFF database (R040050), proved that this stone was in fact spodumene.

Pure spodumene is colorless. Various colors may result from the presence of trace elements such as manganese, chromium, and iron, or sometimes from unstable color centers in its crystal structure. When mined, spodumene sometimes emerges from the ground with a blue-violet or green color that can be unstable in light and fade to pink in a relatively short time, sometimes in a matter of hours. This

Figure 22. The blue spodumene's Vis-NIR spectrum showed bands at 543 and 637 nm that are responsible for its color.



suggests that the spodumene crystals have been exposed to some natural source of radiation (K. Nassau, *Gemstone Enhancement*, Butterworth-Heinemann, London, 1984, pp. 162–163). Blue spodumene has also been reported to result from artificial irradiation (G. Bosshart et al., "Colorimetric investigation of unstable and stable spodumene colours," *International Gemmological Conference 2011 Proceedings*, Interlaken, Switzerland, pp. 26–30). The Vis-NIR spectrum (figure 22) shows the bands at 543 and 637 nm, which are responsible for the blue color of the stone.

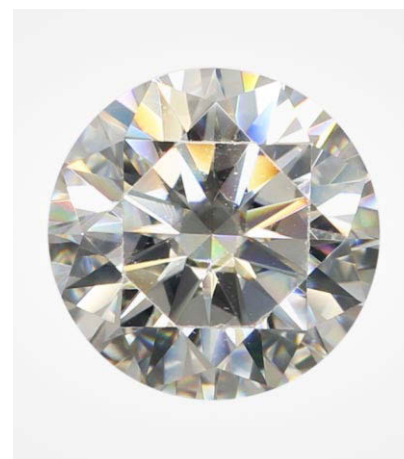
The main source of gem-quality spodumene is Afghanistan; other sources are Pakistan, Brazil, Madagascar, Mozambique, and the United States. While it is unknown whether the color of this blue spodumene was of natural or artificial origin, such stones are rarely seen as faceted gems, and this unusual large example would be of interest to any gem collector.

Forozan Zandi

### SYNTHETIC MOISSANITE with Fraudulent GIA Inscription

GIA Johannesburg recently received a 1.02 ct round brilliant (figure 23) for a

Figure 23. This 1.02 ct round brilliant with a fraudulent GIA inscription proved to be synthetic moissanite.



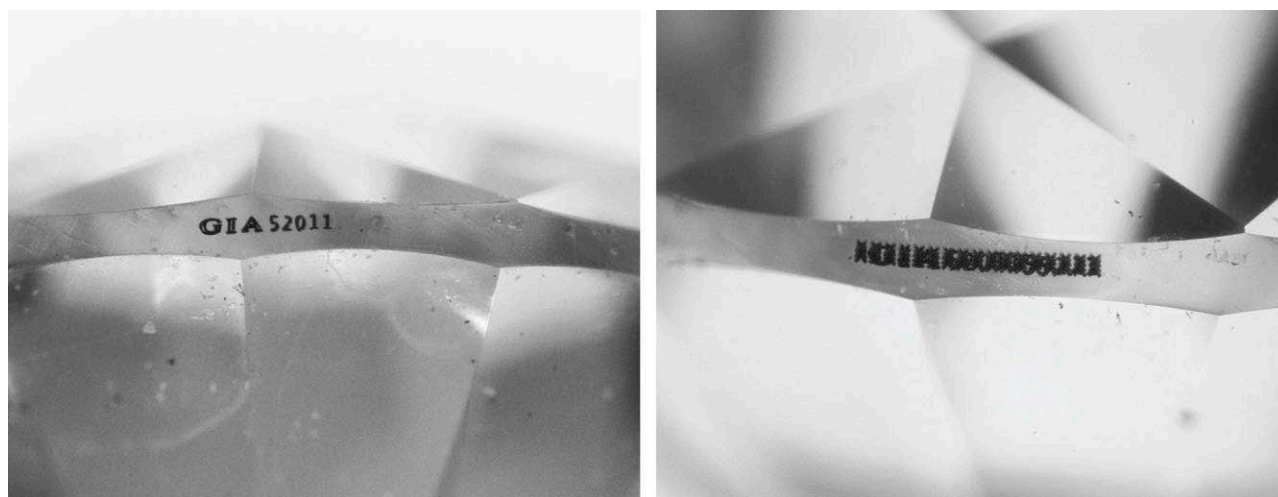


Figure 24. Left: The fraudulent inscription observed on the synthetic moissanite (the GIA report number is partially redacted in this photo for privacy). Right: GIA's standard procedure in these instances is to obscure the fraudulent inscription so it is no longer legible.

Diamond Grading report. Standard testing showed it was not a diamond, and subsequent spectroscopic and gemological analysis proved it to be synthetic moissanite. We often encounter simulants submitted for diamond grading, and they are easily detected through the standard grading process. This near-colorless synthetic moissanite was noteworthy because it had a fraudulent GIA inscription. GIA checks all stones with a preexisting inscription, and this one was obviously not inscribed by GIA. The report number does belong to an E-color natural diamond graded in 2019 with the same weight. But because of the dissimilar SGs of diamond and moissanite (3.52 and 3.22, respectively), their measurements were quite different.

Furthermore, the fraudulent inscription (figure 24, left) was distinctly different from GIA's standard inscription font. GIA's standard practice in such cases is to superimpose characters to obscure the original inscription (figure 24, right). The clarity would have been equivalent to VVS<sub>2</sub> (if such clarity grades were assigned to synthetic moissanite), while the clar-

ity of the graded natural diamond was VVS<sub>1</sub>. The synthetic moissanite did not have any distinguishing inclusions, but it did show obvious double refraction in the microscope. Both IR absorption and Raman spectra confirmed the identification as synthetic moissanite.

In recent years, GIA has encountered similar instances of fraud. One was a synthetic moissanite that had been fashioned to resemble a natural rough diamond octahedron (Winter 2017 Lab Notes, pp. 462–463). That same year, an HPHT laboratory-grown diamond was submitted with a fraudulent inscription corresponding to a natural diamond (Fall 2017 Lab Notes, p. 366). However, this is our first instance of a fraudulent inscription on a diamond simulant.

Synthetic moissanite (SiC) is sometimes mistaken for diamond because some of its properties approach those of diamond, namely hardness and thermal conductivity (a trait measured in some instruments to distinguish diamond from many other simulants). However, several other properties are quite different from diamond, such as a much higher dispersion (leading to

more obvious fire) and double refraction. Nevertheless, the possibility exists that a consumer could purchase this simulant thinking it was a natural diamond, especially with a deliberately misleading inscription. In this case, careful examination protected the consumer against such attempted fraud.

*Authors' note: Since the writing of this lab note, GIA Johannesburg has received and identified two more synthetic moissanites with fraudulent GIA inscriptions. They were handled in a similar manner.*

*Sicebiso Hlatshwayo and  
Sally Eaton-Magaña*

#### PHOTO CREDITS

Nuttapol Kitdee—1; Vararut Weeramongkhonlert—2; Diego Sanchez—4, 11, 13, 20; Nathan Renfro—6; Shunsuke Nagai—9, 17; Taku Okada—10; Britni LeCroy—12, 15 (right); Artitaya Homkrajae—14, 15 (left, center), 16; Masumi Saito—18; Innocentia Nzuza—23; Tuan Grieznel—24